

**A Monte Carlo radiative transfer model of gas-embedded stellar systems
integrated in MUSE**

Authors:

Evangelos Angelou, Andrea Sottoriva

Supervisor:

Prof. Simon Portegies Zwart

Universiteit van Amsterdam, The Netherlands

June 13th, 2008

Contents

1	Introduction	5
2	Monte Carlo for Radiative Transfer	7
2.1	History of Monte Carlo methods	7
3	Radiation transfer: theoretical background	9
3.1	Basic concepts	9
3.2	Photon generation and propagation	9
3.3	Scattering and absorption	10
3.4	Mean Intensity, Flux and Radiation Pressure	10
4	The plane parallel slab	11
4.1	Scenario	11
4.2	Isotropic scattering	12
4.2.1	Validation	12
4.2.2	Results and measures	13
4.3	Anisotropic scattering	16
4.3.1	Theoretical background	16
4.3.2	Dust scattering	18
4.3.3	Validation	19
4.3.4	Results and measurements	20
4.3.5	Gas scattering	21
5	3-dimensional Cartesian grid	23
5.1	Basic concepts	23
5.2	Integration	23
5.3	Results and experiments	23
6	Radiative transfer integrated in the multiscale simulation environment MUSE	25
6.1	MUSE: Multiscale Multiphysics Scientific Environment	25
6.2	Handling multiple point sources with variable luminosity	25
6.3	The interstellar medium distribution	26
6.4	A lightweight radiative transfer module for MUSE	26
6.5	Results	27
7	Conclusions	29

1 Introduction

Monte Carlo methods for radiative transfer are nowadays well known and widely used in both Astronomy and Physics. The idea behind those techniques is very simple: simulate the trajectory of a large number of photons keeping track of their interaction with the underlying interstellar medium. For a sufficient number of simulated particles such methods have proved to be as accurate as their analytical counterpart. Moreover, Monte Carlo simulations allow us to model systems with an arbitrary distribution of the interacting material (e.g. dust or gas).

In order to understand the meaning of the detailed images produced by modern telescopes, the finest models for radiation transfer become necessary and Monte Carlo methods are a suitable candidate for this task. We have investigated the phenomenon of radiation transfer on dust and gas embedded stellar systems using Monte Carlo methods. We will discuss several aspects of radiative transfer and we will show the results we obtained. Finally the code has been integrated in *MUSE*¹, a massive stellar system simulation software.

¹<http://muse.li>

2 Monte Carlo for Radiative Transfer

The concept of Monte Carlo radiation transfer is extremely easy: we generate a new photon from a defined light source (a star) and we let it travel for a certain length, until it interacts with the interstellar medium (gas or dust).

The system consists of a star producing photons isotropically and a certain amount of dust and/or gas between the observer and the light source that influence the trajectories of the emitted photons.

Once the photon is generated, two important phenomena may happen along the its path:

- Scattering

The trajectory of the particle is deviated according to a certain probability distribution and depending on the type of scattering (electron scattering, dust scattering, ...) and many other factors.

- Absorption

The photon is absorbed by the matter, the journey is over.

Finally, by projecting all the surviving photons onto the observer's plane, it is possible to generate images.

2.1 History of Monte Carlo methods

Monte Carlo methods are known from the beginning of the 20th century, when they were generically called *statistical sampling*. The name *Monte Carlo* refers to their randomness and repetitiveness, characteristics in common with the famous *casino* of Monaco.

Such a fancy name became popular thanks to famous physicists like *Stanislaw Ulam*, *Enrico Fermi*, *John von Neumann* and *Nicholas Metropolis*. The story narrates that Ulam's uncle, a well-known hardcore gambler, would constantly borrow money from friends and relatives because he "just had to go to Monte Carlo". From there the name *Monte Carlo methods* proposed by Ulam[1].

Probably the most famous early use of Monte Carlo techniques was by Enrico Fermi during his studies in Rome on the *moderation of the neutron*. There he was performing Monte Carlo calculations using mainly a small mechanical adding machine. Afterward, while working in the ENIAC operation in Los Alamos, Fermi persuaded his friend and collaborator Percy King to build an improved and ingenious version of his old adding machine. Such instrument was called *FERMIAC* or Monte Carlo *trolley* (Figure 1) and it was used to determine neutrons collision paths in numerous nuclear systems[1].

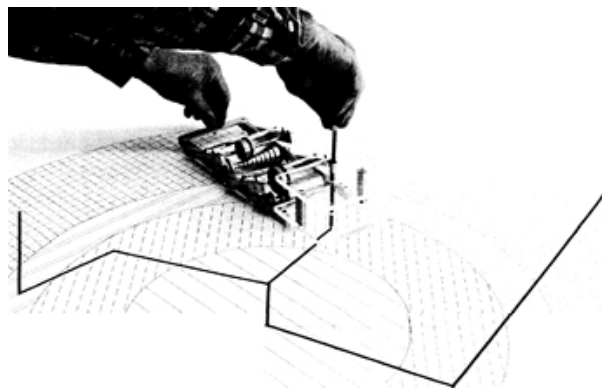


Figure 1. The FERMIAC

Thereafter, Monte Carlo methods played (unfortunately) a central role in the *Manhattan* project and in the successive atomic bombs experiments, when they started to become more and more famous in other fields of science and in business. Monte Carlo techniques have been also important for the development of better and more efficient random number generators. They led to the creation of the *linear congruential generators*, a necessary alternative to the random number tables used until the '50s.

3 Radiation transfer: theoretical background

Here we will introduce some basic concepts of radiative transfer, just necessary to understand the processes we are modeling.

3.1 Basic concepts

Considering a unit surface dA at an angle θ to its normal, within a solid angle $d\Omega$ and a frequency range $d\nu$ in a time interval dt , the intensity I_ν is defined with respect to the radiant energy dE_ν as:

$$I_\nu = \frac{dE_\nu}{\cos\theta dA dt d\nu d\Omega} \quad (1)$$

It is measured in [$ergs cm^{-2} s^{-1} Hz^{-1} sr^{-1}$] and denotes the radiation energy (within a certain frequency) crossing a certain area with a certain direction per second. Another important term, the flux F_ν , is the energy that crosses an area dA per unit of time:

$$F_\nu = \int I_\nu \cos\theta d\Omega \quad (2)$$

measured in [$ergs cm^{-2} s^{-1} Hz^{-1}$].

Those two terms play a central role in the process of radiation transfer.

Furthermore, being the cross section σ the likelihood of interaction between the photons and the particles in the medium, the energy removed per second per frequency per solid angle from the direction of travel (by either scattering or absorption) is:

$$E_r = I_\nu \sigma \quad (3)$$

Considering then the cross section and the density n of the material, the differential intensity along a length dl is:

$$dI_\nu = -I_\nu n \sigma dl \quad (4)$$

the solution of this differential equation is easily derived as:

$$I_\nu(l) = I_\nu(0) e^{-n\sigma l} \quad (5)$$

Concluding, with ρ the mass density of scatterers and absorbers and κ the opacity of the medium, the following relation stands:

$$n \sigma = \rho \kappa \quad (6)$$

Where $\frac{1}{n \sigma}$ is the average distance that the photon travels between interactions.

We will now study the generation and propagation of the photons throughout the interstellar medium.

3.2 Photon generation and propagation

Having a source S_0 in (x_0, y_0, z_0) we generate N_0 photons γ with initial position $\gamma_0 = (x_0, y_0, z_0)$, zenith angle $\theta_0(-\frac{\pi}{2}, \frac{\pi}{2})$ and azimuth angle $\phi_0(0, 2\pi)$ (we generate only forward-going photons, that are the ones we are interested in). Supposing L the maximum depth of the dusty medium we discretize such length into N steps of size dl .

At each step the probability for a photon to interact along the distance dl is:

$$P_i = n \sigma dl \quad (7)$$

Therefore for N steps and $dl = L/N$ the probability to travel without any interaction yields to the exponential series:

$$P(L) = \left(1 - n \sigma \frac{L}{N}\right)^N = e^{-n\sigma L} = e^{-\tau} \quad (8)$$

Which is just the *pdf* of L and where τ is the *optical depth* along a distance L (number of photons mean free paths along such distance) and it is equal to:

$$\tau = \int_0^L n \sigma dl \quad (9)$$

The *optical depth* τ is an important factor in radiative transfer. It is a measure of total transparency and it is analytically convenient because it unifies the main characteristics of an homogeneous semi-infinite object (depth, density and opacity).

3.3 Scattering and absorption

Once the photon has traveled a distance L , if it is still located inside the interacting dust cloud, either scattering or absorption will occur. The probability that whether the first or the second phenomenon will happen depends on the *albedo* of the medium. The albedo a is simply defined as the probability for a photon to scatter with respect to the total probability (of scatter and be absorbed):

$$a = \frac{n_s \sigma_s}{n_s \sigma_s + n_a \sigma_a} \quad (10)$$

By setting $a = 1$ we have total scattering while by setting $a = 0$ we have total absorption.

3.4 Mean Intensity, Flux and Radiation Pressure

The *mean Intensity* J , the *mean Flux* H and the *mean Radiation Pressure* K are very important astrophysical measures. They are also called *intensity moments* and they are used to measure the thermodynamical and mechanical forces acting throughout the dusty medium. They are defined as:

$$J = \frac{1}{4\pi} \int I d\Omega \quad (11)$$

$$H = \frac{1}{4\pi} \int I \cos(\theta) d\Omega \quad (12)$$

$$K = \frac{1}{4\pi} \int I \cos^2(\theta) d\Omega \quad (13)$$

We have well known theoretical solutions for those values, hence they represent a strong validation measure for the model we have implemented and we therefore will use it to prove it.

See [2] and [3] for more details on radiative transfer theory.

4 The plane parallel slab

4.1 Scenario

We now model the simple case where between the source and the observer there is a plane parallel, uniform, homogeneous and semi-infinite slab of dust. The scenario is depicted in Figure 2.

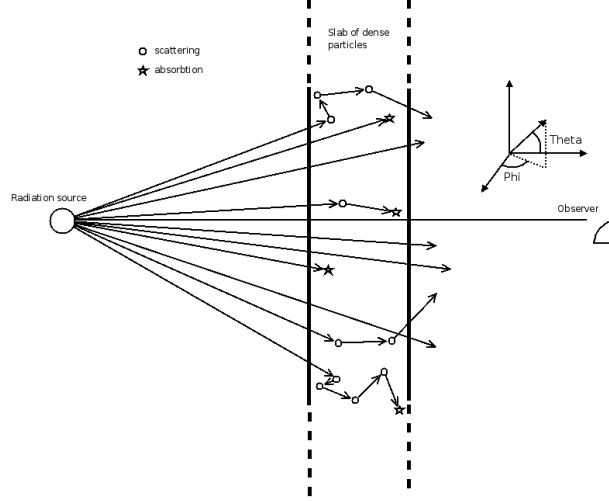


Figure 2. Plane parallel slab

In this case, the probability for a photon to interact before reaching the slab is zero, hence we neglect the empty space between the light source and the slab and we generate photons isotropically directly from the source-side surface border of the slab.

For sake of simplicity we will assume the slab to have always depth of 1.0 and different configurations of maximum optical depth τ_{max} (so different configuration of ρ and κ).

The density ρ and the opacity κ are considered to be homogeneous across the space, we can therefore sample the length that a photon travels from (8) with the inversion method of (14).

$$l = -\frac{\ln(\xi)}{n \sigma} \quad (14)$$

With ξ our uniform random number generator in $(0, 1)$. Simplifying, we can parametrize the slab by its total vertical optical depth $\tau_{max} = n \sigma z_{max}$ (with z_{max} the total the depth of the slab). We would then sample the optical depth τ as:

$$\tau = -\ln(\xi) \quad (15)$$

And we would normalize it to τ_{max} obtaining l with:

$$l = \frac{\tau z_{max}}{\tau_{max}} \quad (16)$$

The corresponding pseudo-code of the MC algorithm is the following:

Algorithm 1. The algorithm for the processing of each simulated photon

```
for all Total number of photons do  
  Generate a new photon from the source  
  while Photon is inside the slab do  
    if rand[0,1] > albedo then  
      Scatter the photon  
    else  
      Absorb the photon  
    end if  
    Compute thermodynamical measures  
  end while  
  Project the photon into the observer's viewplane  
end for
```

4.2 Isotropic scattering

The simplest scattering technique is the *isotropic scattering*. It consists of having a uniform probability distribution of the scattering angles $\theta \in (0, 2\pi)$ and $\phi \in (0, \pi)$.

This models an ideal case and it cannot represent real dust scattering where, as we will see further, the scattering is not isotropic and it depends on the incident angle of the photon at the moment of the interaction.

4.2.1 Validation

Isotropic scattering is a simple approximation of the reality, nevertheless it is well studied and analytical solutions for some measures of the system are available from the literature.

The most important validation measure is the relation between the incident θ angle of the photons and the normalized total intensity I . The results are shown in Figure 3 where the solid line corresponds to the analytical solution (Chandrasekhar [3] 1960) and the points are the Monte Carlo simulation (see [2], Figure 1a).

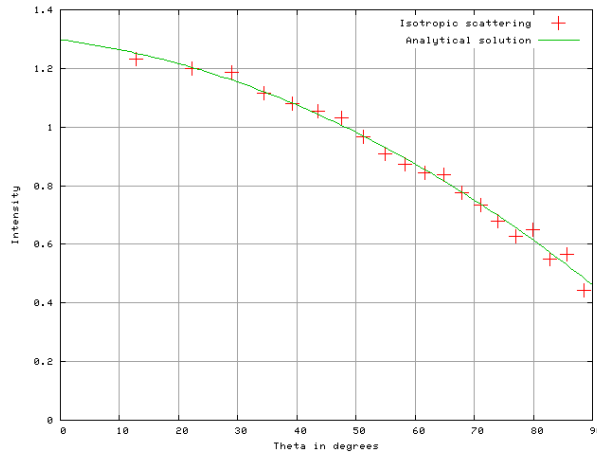


Figure 3. Total intensity I for a plane slab with $\tau_{max} = 10$ and $a = 1$, against the exiting θ angle (single run: 100K photons)

As we discussed previously, another strong validation measure are the intensity moments J, H, K. In order to calculate them for a plane parallel structure we divide the slab into n parallel slices, orthogonal to the viewing plane. We then compute the moments for each slice and we finally plot the J, H, K values across the slab using the discretized formulae:

$$J = \frac{B_\nu}{4N_0} \sum_i \frac{1}{|\mu_i|} \quad (17)$$

$$H = \frac{B_\nu}{4N_0} \sum_i \frac{\mu_i}{|\mu_i|} \quad (18)$$

$$K = \frac{B_\nu}{4N_0} \sum_i \frac{\mu_i^2}{|\mu_i|} \quad (19)$$

Where B_ν is the *total flux* and N_0 is the total number of photons we generate. The results are shown in Figure 4.

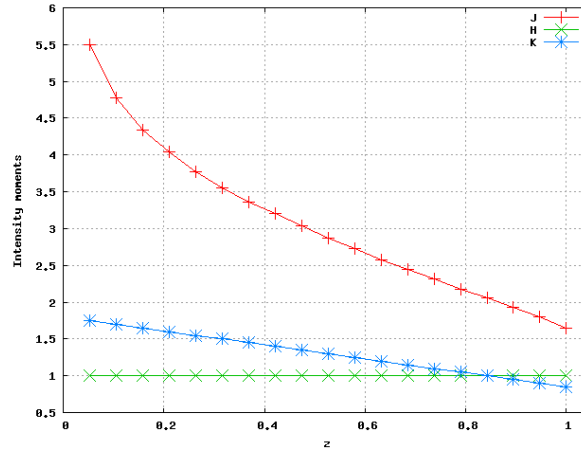


Figure 4. Intensity moments for a plane slab with $\tau_{max} = 10, a = 1$

The data we obtained are coherent with [2] (Figure 1b). Once validating the model, we can perform several interesting experiments and measures with it, as described in the following section.

4.2.2 Results and measures

Using isotropic scattering we can conduct simple but interesting experiments: we generate 10M photons from a point source through a slab of maximum optical depth $\tau_{max} = 10$. Figure 5 shows the variation of the intensity I for different values of *albedo* (0.6, 0.8, 1.0) respectively.

The relation between the intensity and the albedo resulted from the simulation is depicted in Figure 6. As it appears from picture 5 and 6 the intensity that reach the observer seems to increase exponentially with the albedo.

We suppose that is because along a path L_k with k average interactions, the probability to avoid absorption is $(1 - a^k)$ and such polynomial term is increased by the several other factors induced by the scattering process.

From another perspective, linear variations of the medium density ρ lead to linear variations of the optical depth τ . As we sample the non-interaction length L from $-\frac{\ln(\xi)}{\rho\kappa}$, we expect L to decrease like ρ^{-1} , decreasing in

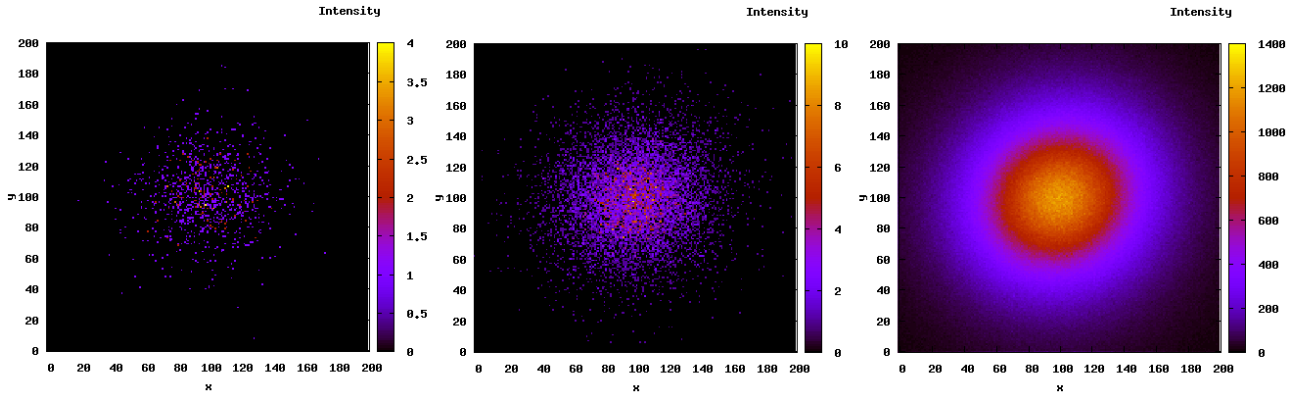


Figure 5. Intensity for $\tau_{max} = 10$, 10M photons and albedo of 0.6, 0.8 and 1.0 respectively.

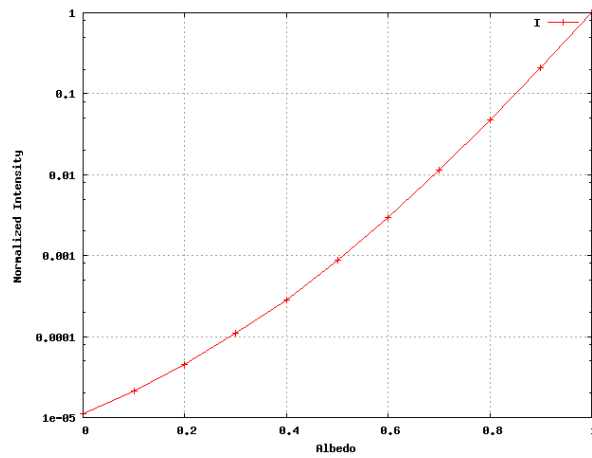


Figure 6. Total normalized intensity for $\tau_{max} = 10.0$, 1M photons, and variations of albedo (logarithmic scale in y)

this way the signal/noise ratio $\frac{S}{N}$. In particular we found a logarithmic relation between the total intensity I that reaches the observer and the slab density ρ (so the optical depth τ). Such relation is expressed by Figure 7.

The exiting photons, appropriately projected into the observer's frame are shown in Figure 8 for 10M photons and albedo 1.0.

Using a constant scale as in Figure 9 it is more clearly what it would be visible of the stellar system by an eventual telescope if increasing the optical depth (a denser dust layer).

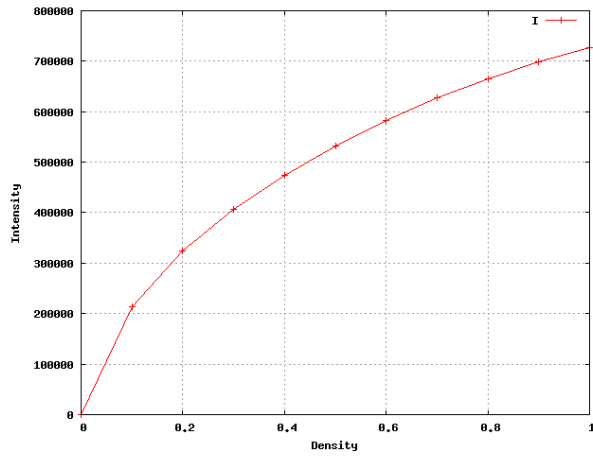


Figure 7. Intensity values with respect to variations of τ_{max} (1M photons, 1.0 albedo)

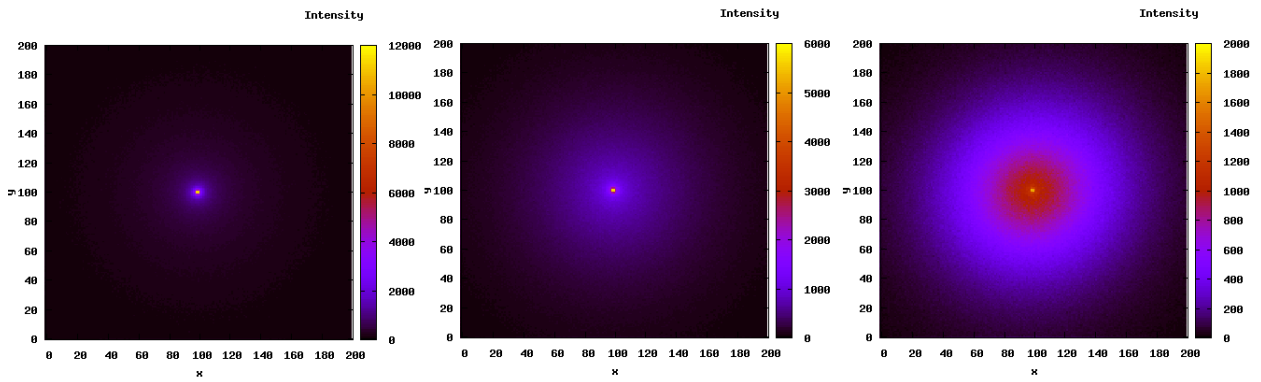


Figure 8. Intensity for $\tau_{max} = 1.0$, $\tau_{max} = 2.5$ and $\tau_{max} = 5.0$ respectively.

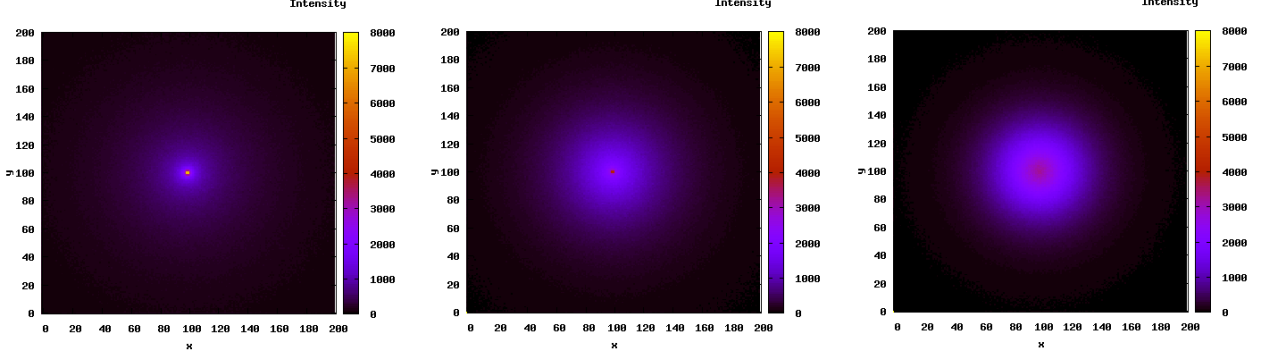


Figure 9. Intensity for $\tau_{max} = 1.0, \tau_{max} = 2.5, \tau_{max} = 5.0$ respectively with constant scale

4.3 Anisotropic scattering

The 99% of the interstellar material is composed by gas and the rest by dust. Nevertheless in some cases dust plays an important role and modeling it becomes of interest. An example are nebula or some types of *accretion discs* found in binary star systems or AGN (active galactic nuclei). The dust particles are usually irregular in shape and they are composed by mostly silicates, carbon, ice and/or iron compounds while the gas present in interstellar medium such as molecular clouds is mostly molecular hydrogen. We will present one scattering algorithm for dust and one for gas and we will show the relative results for both scenarios.

4.3.1 Theoretical background

Isotropic scattering with no polarization is not a good approximation for many problems. Using instead *Rayleigh* scattering and the *Henyey-Greenstein* [4] phase function we are able to approximate dust scattering.

Rayleigh scattering happens when the scattering particles are smaller than the wavelength of the light crossing them, for example in the Earth's atmosphere (where *Rayleigh* scattering causes the typical blue color of the sky).

For anisotropic scattering the new scattering angle is obviously not uniformly distributed, but depends on the incident angle of the photon at the moment of the interaction and on several others parameters. Moreover the anisotropic scattering algorithm we are using keeps track of the polarization state of each single photon in the system along its path.

The polarization state of an electromagnetic wave depends on the complex amplitudes E_x, E_y of the electric field E along the two axis, orthogonal to the direction of travel. To define the polarization state space of a photon we use the Stokes' parameters [5] (I, Q, U, V) computed with respect to three vector bases: the standard *Cartesian* basis (\hat{x}, \hat{y}), a 45 degrees rotated *Cartesian* basis (\hat{a}, \hat{b}) and a circular base (\hat{l}, \hat{r}) as follows:

- $I \equiv |E_x|^2 + |E_y|^2$
- $Q = I\rho\cos(2\phi)\cos(2\theta) \equiv |E_x|^2 - |E_y|^2$
- $U = I\rho\sin(2\phi)\cos(2\theta) \equiv |E_a|^2 - |E_b|^2$
- $V = I\rho\sin(2\theta) \equiv |E_l|^2 - |E_r|^2$

Where I is the total intensity, Q and U are the linear polarizations relative to the standard basis and the rotated basis respectively, V is the circular polarization. Note that the 2θ and 2ϕ terms model the fact that the polarization

is invariant for rotation of 180° . Figure 10 shows the geometrical meaning of the Stokes' parameters where $(I, Q, U, V) = (S_1, S_2, S_3, S_4)$, while examples of possible polarizations are shown in Figure 11.

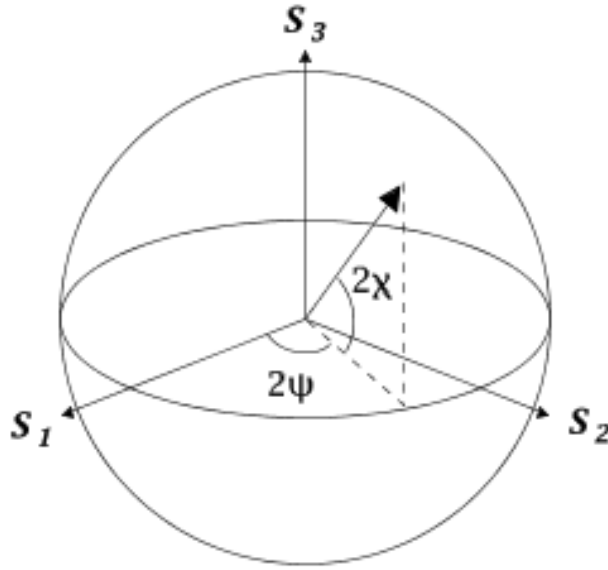


Figure 10. Poincare sphere representing the Stokes parameters

100% Q	100% U	100% V
<p>+Q</p> <p>$Q > 0; U = 0; V = 0$ (a)</p>	<p>+U</p> <p>$Q = 0; U > 0; V = 0$ (c)</p>	<p>+V</p> <p>$Q = 0; U = 0; V > 0$ (e)</p>
<p>-Q</p> <p>$Q < 0; U = 0; V = 0$ (b)</p>	<p>-U</p> <p>$Q = 0; U < 0; V = 0$ (d)</p>	<p>-V</p> <p>$Q = 0; U = 0; V < 0$ (f)</p>

Figure 11. Example of possible polarizations using Stokes' parameters

In our simulation the polarization state of each new photon emitted from the source is initialized to $(1, 0, 0, 0)$ which is the case where we have no initial polarization (in absence of magnetic or electric fields). In other words the likelihood of any polarization state at the photon source is uniform.

Each time a photon scatters its polarization changes and so does its Stokes' vector according to the following equation:

$$S' = L(\pi - i_2)RL(-i_1)S \quad (20)$$

Where the matrix R describes the scattering probability depending on the incident angle of the photon and L is the *Mueller* matrix that rotates towards the coordinates of the observer. In absence of magnetic fields the scattering

matrix R is relatively simple:

$$R(\Theta) = a \begin{pmatrix} P_1 & P_2 & 0 & 0 \\ P_2 & P_1 & 0 & 0 \\ 0 & 0 & P_3 & -P_4 \\ 0 & 0 & P_4 & P_3 \end{pmatrix}$$

While the *Mueller* matrix just rotates the system depending on the observer's frame:

$$L(\psi) = a \begin{pmatrix} 1 & 0 & 0 & 1 \\ 0 & \cos(2\psi) & \sin(2\psi) & 0 \\ 0 & -\sin(2\psi) & \cos(2\psi) & 0 \\ 0 & 0 & 0 & 1 \end{pmatrix}$$

Depending on the kind of scattering we want to model, the matrix above must be filled with different values.

4.3.2 Dust scattering

For dust scattering the matrix R must be filled in with the following values[4]:

$$a = 3/4 \tag{21}$$

$$P_1 = \frac{1 - g^2}{(1 + g^2 - 2g \cos(\Theta))^{3/2}} \tag{22}$$

$$P_2 = -p_l P_1 \frac{1 - \cos(\Theta)^2}{1 + \cos(\Theta)^2} \tag{23}$$

$$P_3 = P_1 \frac{2\cos(\Theta)}{1 + \cos(\Theta)^2} \tag{24}$$

$$P_4 = -p_c P_1 \frac{1 - \cos(\Theta_f)^2}{1 + \cos(\Theta_f)^2} \tag{25}$$

Where:

- g is the scattering asymmetry parameter (0 = isotropic scattering, 1 = forward-throwing)
- p_l is the peak linear polarization
- p_c is the peak circular polarization
- $\Theta_f = \Theta(1 + 3.13se^{-7\Theta/\pi})$, with s the skew factor (taken to be unity as described by [6]).

At this point we solve the system 20 as follows:

- we sample i_1 from a uniform angular distribution ($i_1 = 2\pi\xi$)
- we sample Θ from the scattering matrix R as follows:

$$\cos(\Theta) = \frac{1+g^2 - [(1-g^2)/(1-g+2g\xi)]^2}{2g}$$

- we calculate i_2 and the new scattering angles θ and ϕ (see [3] for the details)
- we then compute the new Stokes' parameters S , in this way we can keep track of the polarization state of the photon along its path.

Having the new angles θ and ϕ we can scatter the photon and we step forward to the next interaction.

4.3.3 Validation

Again as we did for the isotropic scattering we need to validate the model. The *Chandrasekhar* analytical solution however refers only to the isotropic case. Hence we set the scattering asymmetry parameter g to 0 in order to simulate isotropic scattering. We then plot the relation between the normalized intensity I and the exiting θ angle of the photons. The results are shown in Figure 12: the solid line is the *Chandrasekhar* analytical solution while the points are our Monte Carlo code.

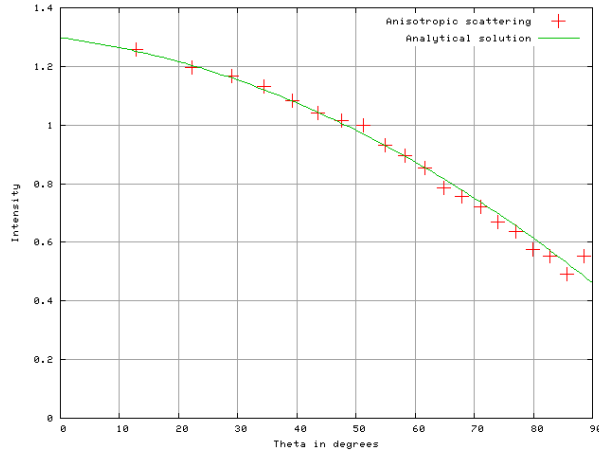


Figure 12. Total intensity I for a plane slab with $\tau_{max} = 10$ against the exiting θ angle (single run: 100K photons)

Finally we again plot the moments J, H and K using the anisotropic scattering algorithm (Figure 13).

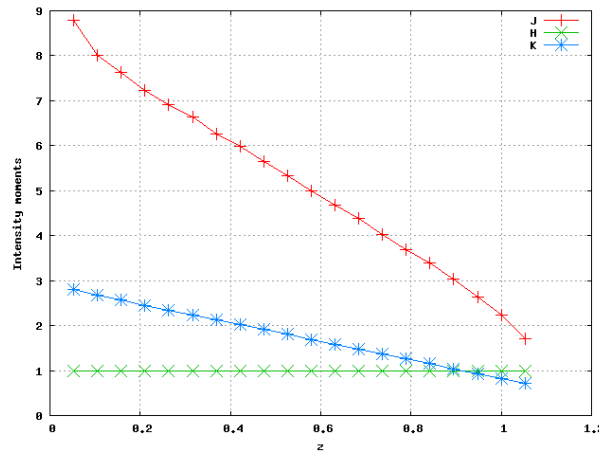


Figure 13. Intensity moments using anisotropic scattering for the *ultraviolet* band and density $\rho = 0.01$ but with $g = 0$ (see table at 4.3.4)

4.3.4 Results and measurements

The properties of interstellar dust (total opacity, albedo, scattering asymmetry parameter and peak linear polarization) are well known and they are available in literature for many radiation bands. Those values, together with the described scattering technique permit us to do very interesting experiments. We simulate a parallel slab with depth 5.0 assuming also constant density of 0.001 and changing the total opacity κ according to the following table.

Band $\lambda(\mu m)$	κ	a	g	p_l
U(0.34)	360	0.54	0.48	0.26
B(0.44)	286	0.54	0.48	0.31
V(0.55)	219	0.54	0.44	0.43
R(0.73)	156	0.53	0.37	0.58
I(0.85)	105	0.49	0.29	0.70
J(1.25)	65	0.43	0.16	0.75
H(1.65)	38	0.33	0.06	0.87
K(2.20)	20	0.21	0.02	0.93

The results in Figures 14 and 15 show how the same stellar system, simulated with 100M photons, appears if seen either through the *ultraviolet* band U or through the *infrared* band K (see 4.3.4).

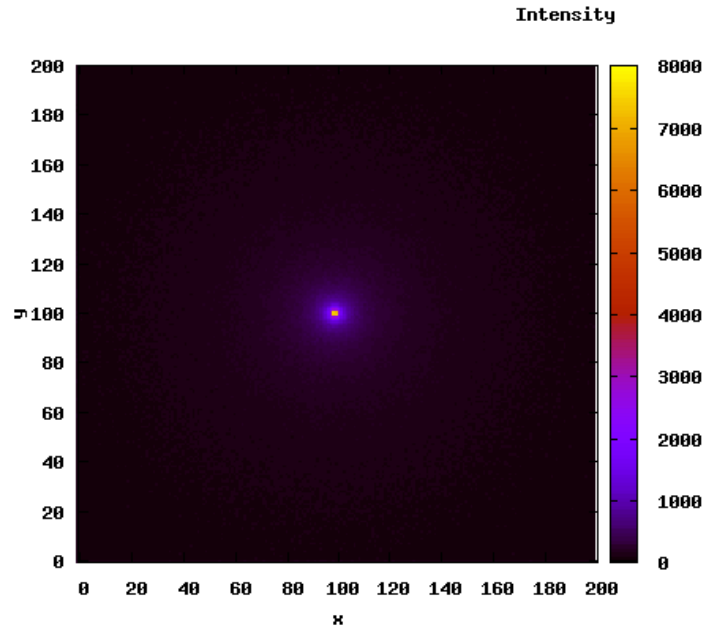


Figure 14. Intensity for the ultraviolet band U

Although the ultraviolet band has a higher total opacity, the albedo is more than a half of the albedo of the infrared band. Moreover the scattering in the infrared is almost isotropic while the asymmetry parameter for the ultraviolet band is 24 times larger.

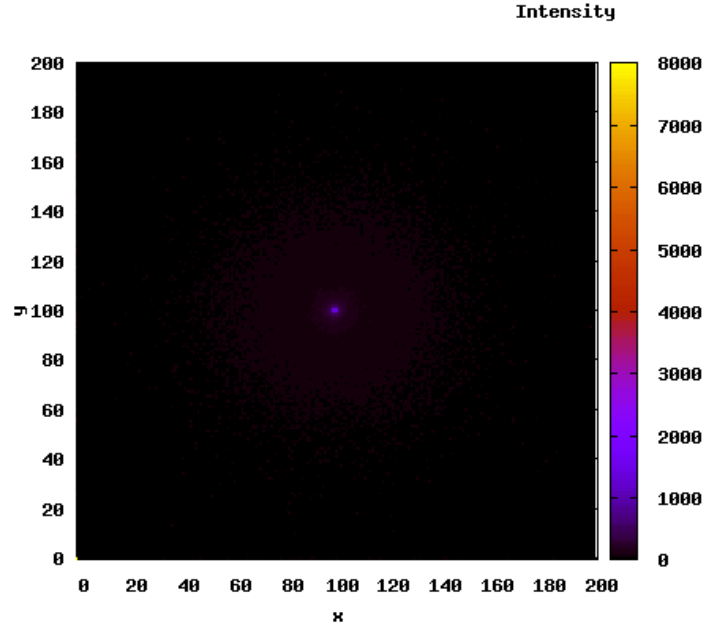


Figure 15. Intensity for the infrared band K

4.3.5 Gas scattering

As outlined before, considering that 99% of the interstellar medium is composed by gas (mostly molecular hydrogen), a gas scattering algorithm is another interesting topic to discuss. We consider *electron scattering* as the main form of scattering process and we model it using the theoretical framework previously discussed but filling the scattering matrix R as follows:

$$a = 3/4 \quad (26)$$

$$P_1 = \cos^2(\Theta) + 1 \quad (27)$$

$$P_2 = \cos^2(\Theta) - 1 \quad (28)$$

$$P_3 = 2\cos(\Theta) \quad (29)$$

$$P_4 = 0 \quad (30)$$

With the scattering distribution:

$$D = P_1 I + P_2 \cos(2i_1) Q - P_2 \sin(2i_1) U \quad (31)$$

In order to sample from the above distribution we use the rejection method in the following way:

- Sample Θ from a uniform distribution $\cos(\Theta) = 1 - 2 * \xi$
- Compute D from the above equation

- If $\xi < D/2$ (peak value for D is 2) then continue with the scattering angle Θ otherwise choose another

This type of scattering will be used in the multiple point source examples with the version of our code integrated in MUSE.

5 3-dimensional Cartesian grid

5.1 Basic concepts

In order to simulate a variety of dust clouds around a point source it is necessary to discretize the space. In this way, clouds of different densities and shape can be created, where every cell contributes differently to the optical depth. The space is discretized in each direction to $xdim \cdot ydim \cdot zdim$ grid cells and $(xdim + 1) \cdot (ydim + 1) \cdot (zdim + 1)$ cell faces where each cell has a defined opacity value $\rho_{x,y,z}$.

Therefore, we can no longer approximate the $n\sigma$ term to a constant value as for the plane parallel slab. Each time we generate or we scatter a photon we must instead compute the integral of the opacity along its path until the edges of our grid as explained by 9. We will use such value to sample the new L as in 14. With such grid we can just decide which kind of configuration of interacting medium we want and simulate its distortion effect on a light source.

5.2 Integration

The integration technique used to calculate the randomly sampled optical depth of each run τ traces the course of the photon through the grid. For each cell face that the photon crosses (in x, y or z direction) the corresponding contribution of this cell to the total τ traveled is computed. This means that the contribution of the cell crossed to the total τ of the particular run is the actual distance traveled through the cell multiplied by the cell's density.

The distance to the next cell faces along the propagation unit vector (n_x, n_y, n_z) is calculated using:

$$s_x = \frac{xface - x}{n_x}, s_y = \frac{yface - y}{n_y}, s_z = \frac{zface - z}{n_z} \quad (32)$$

It is reasonable that the photon will hit the minimum of these distances first. The integration process is over when $\tau_{run} + \tau_{cell} > \tau$. When this happens, the photon scatters into the cell at a distance

$$s = \frac{(\tau - \tau_{run})}{\rho_{cell}} \quad (33)$$

5.3 Results and experiments

For all our experiments we were using a grid which discretizes a cubic continuous space of 1.0x1.0x1.0. The first experiment we conducted is the simulation of a uniform and homogeneous cube of dust of dimensions 10x10x10 grid points placed in front of the source at position $-7x7x100$ as shown in Figure 16 (using 200x200x200 grid points).

The asymmetrical position of the cube permits to notice clearly the boundary effects. Our interpretation of this phenomenon is that in the side faces of the cube the density of each projected point is a contribution of many points in the surface of the cube (due to the perspective projection).

Another interesting experiment we performed consisted of simulating the case where we have a star in the middle of an oblate spheroid described by:

$$x^2 + \frac{y^2}{c} + z^2 = r \quad (34)$$

with the opacity that goes with the distance from the center:

$$\kappa = e^{-2r_i/r} \quad (35)$$

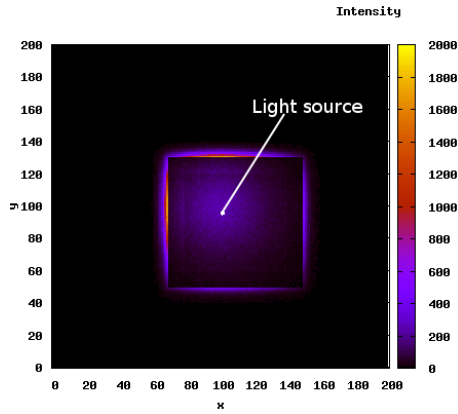


Figure 16. Intensity for a cube of dust placed in front of the source with 200x200x200 grid points

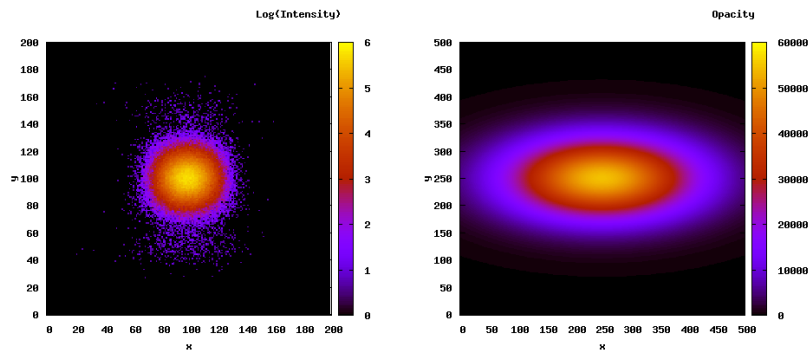


Figure 17. Right: intensity of a spheroid dusty cloud using 2M photons and $a=1.0$. Left: medium density distributed as an oblate spheroid of dust (500x500x500 grid points)

and with $c = 5$. The total opacity κ is depicted in Figure 17 (right) while the results we obtained are shown in Figure 17 (left).

As it can be seen, still we notice the boundaries of the structure. It is anyway interesting to study the influence of the distribution of density in the final image. Also further comparisons against real images could be use for additional validation of the code.

Concluding, the Cartesian grid offers a simple and clean method to simulate complex shapes of dusty material but at the same time needs a huge amount of memory (we could simulate up to 500x500x400 of grid points).

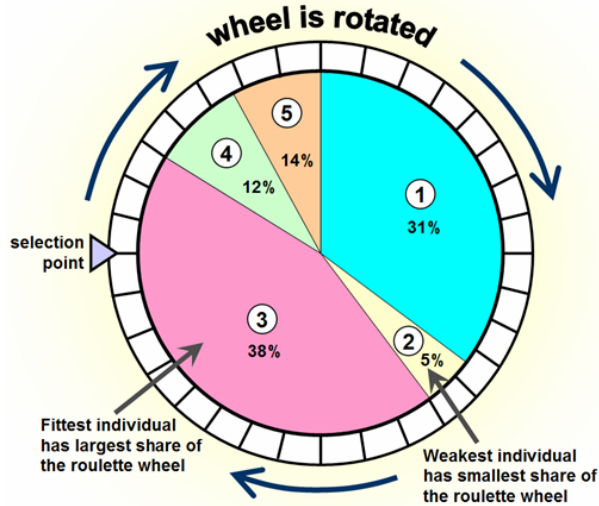


Figure 18. Roulette wheel approach for photons sharing: selection based on “fitness”, in our case replaced by the star luminosity[10].

6 Radiative transfer integrated in the multiscale simulation environment MUSE

6.1 MUSE: Multiscale Multiphysics Scientific Environment

MUSE[9] is a multiphysics environment able to simulate dense stellar systems such as globular clusters and galactic nuclei. Its aim is to provide a coherent and flexible interface for different simulation softwares such as *stellar dynamics*, *stellar evolution* and *hydrodynamics* to work together through a set of easy-to-use *python* interfaces. The idea is to address the multiscale problem of dense stellar systems simulation using an highly modularized architecture. In such ways all the parts of the simulation (defined as *modules*) can be combined together, allowing the user to easily build the simulation chain, substitute a specific module or create a new one. Those modules can be written in any programming language and once compiled, the object files will communicate using simple, user-defined, *python* interfaces. This kind of approach proved to be very efficient on handling the complexity of the problem. It was also very simple for us to port our code into MUSE and use it coherently with all the other modules already available inside the MUSE framework.

6.2 Handling multiple point sources with variable luminosity

In order to simulate the radiative transfer of dense stellar systems it is necessary to handle multiple point sources. The same principle that is used to simulate the photon scattering can be expanded to multiple point sources using nothing more than an accurate description of the initial star positions within a discretized space. Using the MUSE interfaces, the radiative transfer module gets the information about stars positions from the stellar dynamics code and about their luminosities from the stellar evolution one. The total number of photons to simulate will be shared according to the luminosity of each star using a *roulette wheel* approach as shown in Figure 18.

The Roulette Wheel technique is implemented using a stochastic sampling algorithm as seen in Algorithm 2. After the photons partitioning process each of the photons is processed independently as described for the single point source case.

Algorithm 2. The algorithm for photons sharing amongst the stars

```
Add the luminosities of all point sources to total_lum
Draw a random number RAND between 0 and total_lum
for all Stars do
  if RAND - Star.luminosity  $\leq$  0 then
    Break and use Star position as initial for the photon
  end if
end for
```

6.3 The interstellar medium distribution

Once the stars are positioned inside the 3D-cartesian grid, an interstellar medium distribution must be defined, just as outlined in Section 5. Unfortunately the hydrodynamics module is not yet available in MUSE (although it will be soon), hence currently the simulation does not take into the account the interaction between the interstellar medium and the stellar hydrodynamics.

Despite this limitation we can perform realistic experiments by fixing any distribution of gas constant in time. Although not physically accurate such configuration is optimal for validation and can produce images of relevant interest. Nevertheless the final objective remains that of collecting the medium distribution from the hydrodynamics module, and use it in the radiative transfer module at runtime, using MUSE interfaces.

6.4 A lightweight radiative transfer module for MUSE

Our radiative transfer code is actually integrated as a modular component of the MUSE architecture and is available for download from the official website [9]. The software represents a lightweight radiative transfer code as described in Section 3 and 4. It offers the user a useful and interesting visualisation tool for MUSE, able to produce realistic images of the system. The RT module for MUSE mainly provides to the user one simple function call:

```
ComputeRT(stars_array, number_of_stars, cloud_grid, cloud_grid_size [in points],
cloud_dimensions [in pc])
```

The function allows to process a radiative transfer image of the system at any time point during the simulation. As output the radiative transfer module creates an image file *rtshot[N].dat* (with N increasing at each shot) containing the results of the radiative transfer process and a luminosities file *luminosities[N].dat* containing the distribution of the stars and their luminosities.

Although the code aims for ease of use, there is a large number of available control parameters that can be set in order to create as photorealistic images as it is computationally feasible. In short, the user can manipulate:

- The total number of photons to generate (via `SetNumberOfPhotons()`)
- The simulation grid's dimensions and coarseness (via `ComputeRT()`).
- The density and opacity of the stellar gas/dust cloud for each grid cell (via `ComputeRT()`).
- The albedo, that is the ratio of scattered to absorbed photons in each Monte Carlo step (via `SetAlbedo()`).
- The observer's point of view, in terms of distance from the grid back wall and direction of sight in spherical coordinates: ϑ, φ (via `SetObserver()`).

- The type of scattering to use, currently supported are isotropic, dust and electron scattering (via `SetScatteringType()`).
- The output filenames (via `SetOutputFiles()`)
- The random number generator's seed (via `SetRandomSeed()`).

Further information on the usage and current state of the code can be found in the module's manual[11]. It provides a starting point for the user that wants to get started quickly with the module and provides a detailed description of a test program that binds all the different modules together.

6.5 Results

As outlined earlier, the code takes a set of parameters from the other MUSE modules in order to accurately simulate radiative transfer for light of a particular wavelength, emitted from a cluster of stars. The results of experimentations done to ensure the validity of the code in the case of a single star have been presented in detail in Sections 4 - 5.

The tests were performed by linking the stellar evolution module EFT89 and the stellar dynamics module BHTree available from the MUSE trunk with the radiative transfer module, as seen in Figure 19. This ensures that the different modules can be made to work seamlessly through their interfaces. In this case, the simulation is run using a 1024-star Plummer model as the star cluster, with a total star mass of $750 M_{\odot}$ resembling the *Pleiades* star cluster [7]. We will assume the cluster being in the center of a giant molecular cloud with density of $10^2 H_2 cm^{-3}$ as reported in [8]. The scattering parameters are set to simulate visible (red) light, and the results of the simulation are then visualized using the *image* option of gnuplot. The resulting shot is seen in Figure 20 (left) and a simple depiction of the stars positions and luminosities corresponding to the same observer plane is provided in Figure 20 (right).

It is clear that the resulting image depends mainly on two parameters: the star luminosity and the star position inside the medium. The brighter the star, the more photons it generates, therefore it will also appear more bright in the RT image. Nonetheless, the fundamental factor that contributes to the formation of a scattered image is the amount of interstellar medium present between the observer and the star. A linear increase of such distance will produce an exponentially fuzzy image. We therefore expect luminous stars in the back of the grid to produce large fuzz balls and stars close to the observer to generate brighter points with a small dispersion. The result of such interactions can be easily seen in Figure 20 where about a dozen very bright stars dominate the sky, obscuring to the naked eye those less luminous stars that may be closer to the observer. In short, the radiative transfer code is a ready to use module for MUSE which provides a useful visualisation tool for the multiphysics environment and can produce realistic images of large star clusters.

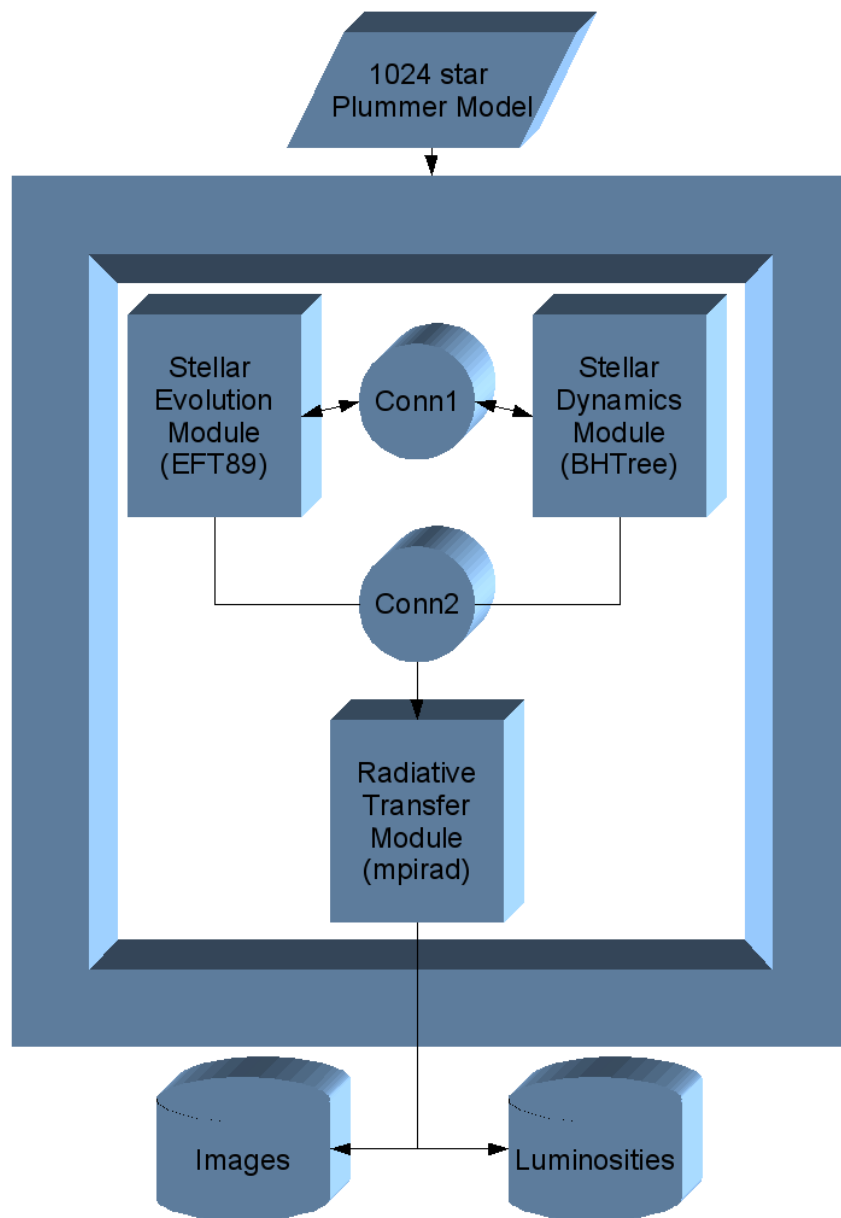


Figure 19. Representation of the interconnections between the different modules in the test program. The 1024 star positions and velocities are passed to the `BHTree` module for the dynamics, while the mass and age of the cluster is handled by the `EFT89` module. `Conn1` represents the connecting routines that transform the output of one module to the others input, i.e. they handle scaling and unit transformations. `Conn2` represents the corresponding transformations on the final output of both modules needed by `mpirad` (that is, star luminosities from `EFT89` and star positions from `BHTree`). The `mpirad` module directly outputs the resulting shots and a map of each simulated star's position and luminosity to help interpret them.

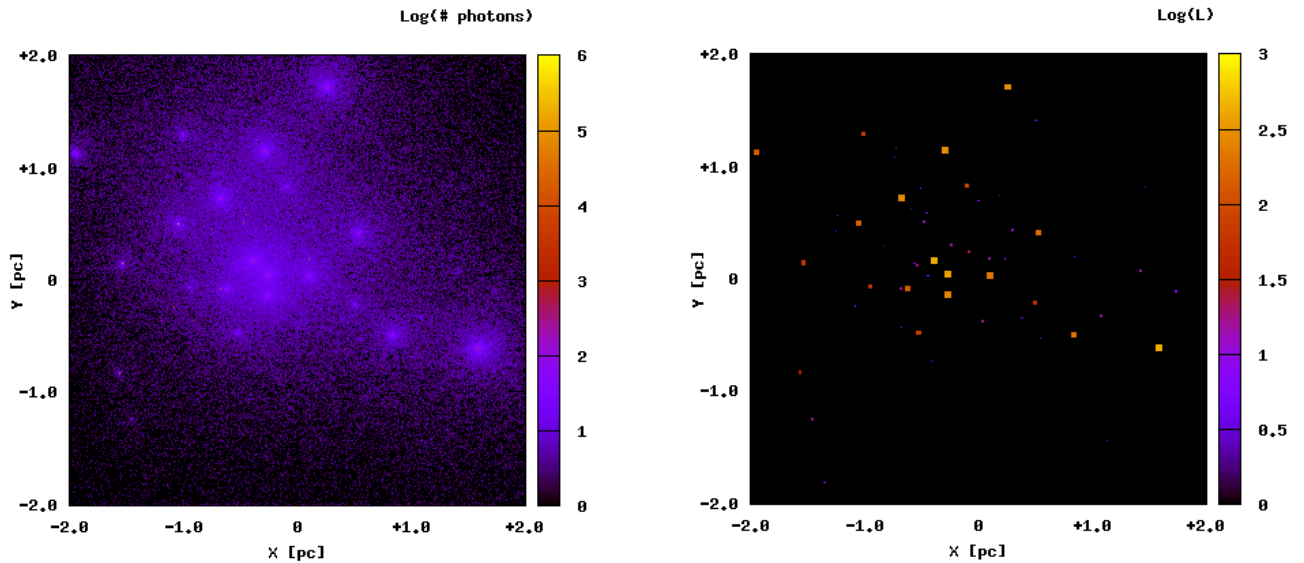


Figure 20. An image after the cluster’s evolution for a time of 120 million years. The image is taken with the observer centered at $[2.0, 1.5, 0.5]$ and with a clipping plane that visualizes a cube of dimensions $4 \times 4 \times 4$ pc. Left: radiative transfer results, right: original luminosities of the stars and their position.

7 Conclusions

The radiation transfer problem is a crucial issue when modeling many astrophysical systems and Monte Carlo methods are particularly suitable for this kind of problem. In this paper we have investigated how we can use Monte Carlo techniques in order to simulate dust and gas radiative transfer. We gave a brief theoretical background and we studied and implemented the different scattering techniques. We discussed a flexible solution using a Cartesian grid for modeling inhomogeneous media and finally presented an interface to our code to provide this kind of functionality as a module of a more general simulation environment like MUSE.

Moreover our implementation can be easily extended to incorporate various complex cloud configurations coming from a future hydrodynamics module in MUSE, using the already developed API. Still, further work is necessary in order to simulate real astrophysical systems, nevertheless the results have been already very interesting and promising.

In conclusion we have shown how to produce quite accurate simulations of radiative transfer for complex stellar clusters, validated our code with experiments against the theoretical solutions and provided the code as a ready to use module of a larger in scope, freely available multiphysics environment.

References

- [1] N. Metropolis (1987),
The beginning of the monte carlo method,
Los Alamos Science Special Issue. 2.1
- [2] K. Wood, B. Whitney, J. Bjorkman, and M. Wolff (2001),
Introduction to monte carlo radiation transfer,
Available: http://gemelli.colorado.edu/~bwhitney/codes/manual_kw.ps. 3.4, 4.2.1, 4.2.1
- [3] Chandrasekhar (1960),
Radiative Transfer,
Dover Publications. 3.4, 4.2.1, 4.3.2
- [4] L.G. Henyey and J.L. Greenstein (1940),
Diffuse radiation in the galaxy,
Astrophysics Journal, 3: 117. 4.3.1, 4.3.2
- [5] H.C. van De Hulst (1981),
Light scattering by small particles,
Dover Publications. 4.3.1
- [6] M.G. White, S.H. Southworth, P.Kobrin, E.D. Poliakoff, R.A. Rosenberg, and D.A. Shirley (1979),
Angular distribution of $xe\ 5s \rightarrow \epsilon p$ photoelectrons near the Cooper minimum,
Physics Review Letters, 43: 1661. 4.3.2
- [7] E. Moraux, P. Kroupa, J. Bouvier (2004),
The Pleiades mass function: models versus observations,
Astron.Astrophys. 426 (2004) 75-80. 6.5
- [8] J.P. Williams, L. Blitz, C.F. McKee (2000),
The Structure and Evolution of Molecular Clouds: from Clumps to Cores to the IMF,
Protostars and Planets IV: 97. 6.5
- [9] S.P. Zwart *et al.* (2008),
MUSE: Multiscale Multiphysics Scientific Environment,
Available: <http://www.muse.li> 6.1, 6.4
- [10] N.University (2008),
Roulette wheel selection,
Available: <http://www.edc.ncl.ac.uk/highlight/rhjanuary2007g02.php/> 18
- [11] E. Angelou, A. Sottoriva, and S.P. Zwart. (2008),
User's guide: Muse radiative transfer module,
Available: http://www.muse.li/browser/trunk/radiative_transfer/mpirad/manual 6.4